JOURNAL OF AIRCRAFT
Vol. 31, No. 4, July–Aug. 1994

Subsonic Static and Dynamic Stability Characteristics of a NASP Configuration

Richmond P. Boyden,* David A. Dress,† Charles H. Fox Jr.,‡ Jarrett K. Huffman,§ and Christopher I. Cruz¶
NASA Langley Research Center, Hampton, Virginia 23681

Wind-tunnel tests of a National Aero-Space Plane configuration were conducted in the NASA Langley Research Center (LaRC) 7- by 10-Foot High Speed Tunnel. The model used is a LaRC designed blended body configuration. Static and dynamic stability characteristics were measured at Mach numbers of 0.3, 0.6, and 0.8. In addition to tests of the baseline configuration, component buildup tests with a canard surface and a body flap were conducted. The baseline configuration showed positive static stability except at the higher angles of attack at 0.8 Mach number. The baseline configuration has positive damping about all three axes. There was generally good agreement between the in-phase dynamic parameters and the corresponding static data. Also included are comparisons of the experimental damping parameters with results from the engineering predictive code Aerodynamic Preliminary Analysis System (APAS). The APAS damping predictions are good for the roll mode, and only fair for the pitch and yaw modes.

Nomenclature

Static longitudinal data are referred to the stability axis system and the static lateral stability data are referred to the body axis system aligned with water line zero (WL 0) as shown in Fig. 1. The dynamic stability data presented are referred to the body axis system inclined 4.25 deg relative to WL 0. Both the static and dynamic stability balances and stings were offset 4.25 deg from the model centerline to avoid any alteration of the upper aft surface of the model. The origin of the axes was located to correspond to the moment reference position shown in Fig. 2. The model reference length for the pitching moment coefficients is the body reference length of 33.6 in. (see Fig. 2). For the yawing and rolling moment coefficients the reference length is the overall wing span of 12.00 in. The reference area of 161.04 in.^{2} is the theoretical wing planform area (including elevons) with the wing leading edges projected to the centerline of the vehicle. The area of the body flap at the rear of the body and the canard are not included in the reference area.

In the following Nomenclature list a dot over a quantity indicates a first derivative with respect to time.

b	= wing span, ft
C_D	= drag coefficient, (drag/$q_\infty S$)
C_L	= lift coefficient, (lift/$q_\infty S$)
C_l	= rolling-moment coefficient, (rolling moment/$q_\infty Sb$)
C_{l_p}	= $[\partial C_l/\partial(pb/2V)]$, per rad
$C_{l_{\dot p}}$	= $[\partial C_l/\partial(\dot p b^2/4V^2)$, per rad
$C_{l_p} + C_{l_{\dot\beta}} \sin\alpha$	= damping-in-roll parameter, per rad
C_{l_β}	= $(\partial C_l/\partial\beta)$, per deg or rad
$C_{l_{\dot\beta}}$	= $[\partial C_l/\partial(\dot\beta b/2V)]$, per rad
$C_{l_\beta} \sin\alpha - k^2 C_{l_p}$	= rolling moment due to roll-displacement parameter, per rad
C_m	= pitching-moment coefficient, (pitching moment/$q_\infty SL$)
C_{m_q}	= $[\partial C_m/\partial(qL/2V)]$, per rad
$C_{m_{\dot q}}$	= $[\partial C_m/\partial(\dot qL^2/4V^2)]$, per rad
$C_{m_q} + C_{m_{\dot\alpha}}$	= damping-in-pitch parameter, per rad
C_{m_α}	= $(\partial C_m/\partial\alpha)$, per rad
$C_{m_{\dot\alpha}}$	= $[\partial C_m/\partial(\dot\alpha L/2V)]$, per rad
$C_{m_\alpha} - k^2 C_{m_{\dot q}}$	= oscillatory longitudinal-stability parameter, per rad
C_n	= yawing-moment coefficient, (yawing moment/$q_\infty Sb$)
C_{n_r}	= $[\partial C_n/\partial(rb/2V)]$, per rad
$C_{n_{\dot r}}$	= $[\partial C_n/\partial(\dot rb^2/4V^2)]$, per rad
$C_{n_r} - C_{n_{\dot\beta}} \cos\alpha$	= damping-in-yaw parameter, per rad
C_{n_β}	= $(\partial C_n/\partial\beta)$, per deg or rad
$C_{n_{\dot\beta}}$	= $[\partial C_n/\partial(\dot\beta b/2V)]$, per rad
$C_{n_\beta} \cos\alpha + k^2 C_{n_{\dot r}}$	= oscillatory directional-stability parameter, per rad
C_Y	= side force coefficient, (side force/$q_\infty S$)
C_{Y_β}	= $(\partial C_Y/\partial\beta)$, per deg
f	= frequency of oscillation, Hz
k	= reduced-frequency parameter ($\omega L/2V$) in pitch; ($\omega b/2V$) in roll and yaw, rad
L	= body reference length, ft
L/D	= lift-to-drag ratio
M	= freestream Mach number
p, q, r	= angular velocity of model about X_D, Y_D, Z_D system of axes, rad/s
q_∞	= freestream dynamic pressure, psf
S	= reference area, ft^2
V	= freestream velocity, ft/s
X_B, Y_B, Z_B	= body system of axes
X_D, Y_D, Z_D	= body system of axes inclined 4.25 deg relative to WL 0.
X_S, Y_S, Z_S	= stability axes system
α	= angle of attack, deg or rad

Presented as Paper 93-0519 at the AIAA 31st Aerospace Sciences Meeting, Reno, NV, Jan. 11–14, 1993; received June 7, 1993; revision received Sept. 29, 1993; accepted for publication Sept. 29, 1993.

*Aerospace Engineer, High-Reynolds-Number Aerodynamics Branch, Applied Aerodynamics Division, M/S 267. Senior Member AIAA.

†Aerospace Engineer, Supersonic/Hypersonic Aerodynamics Branch, Applied Aerodynamics Division, M/S 287. Senior Member AIAA.

‡Aerospace Engineer, Transonic Aerodynamics Branch, Applied Aerodynamics Division, M/S 295.

§Aerospace Engineer, retired, Transonic Aerodymanics Branch, Applied Aerodynamics Division, M/S 295.

¶Aerospace Engineer, Vehicle Analysis Branch, Space Systems Division, M/S 365. Member AIAA.

β = angle of sideslip, deg or rad
ω = angular velocity, $2\pi f$ rad/s

Model Component Designations
B = body
C = canards
F = body flap
N = nacelle
V = outboard vertical tails
V2 = inboard vertical tails
W = wings

Introduction

As part of the development effort for the National Aero-Space Plane (NASP),[1,2] a program was initiated at the NASA Langley Research Center (LaRC) to measure experimentally the static and dynamic stability characteristics of the blended body configuration designated the test techniques demonstrator (TTD). These results were acquired in the LaRC 7- by 10-Foot High Speed Tunnel at Mach numbers of 0.3, 0.6, and 0.8. Component effects were obtained by testing with and without the wings, vertical tails (both inboard and outboard), canards, nacelle, and body flap. The range of angle of attack was from −4 to 16 deg. In addition to the test results, comparisons of the experimental damping parameters with results from the engineering predictive code Aerodynamic Preliminary Analysis System (APAS)[3,4] are also included. The supersonic dynamic stability characteristics of the TTD have been reported in Ref. 5.

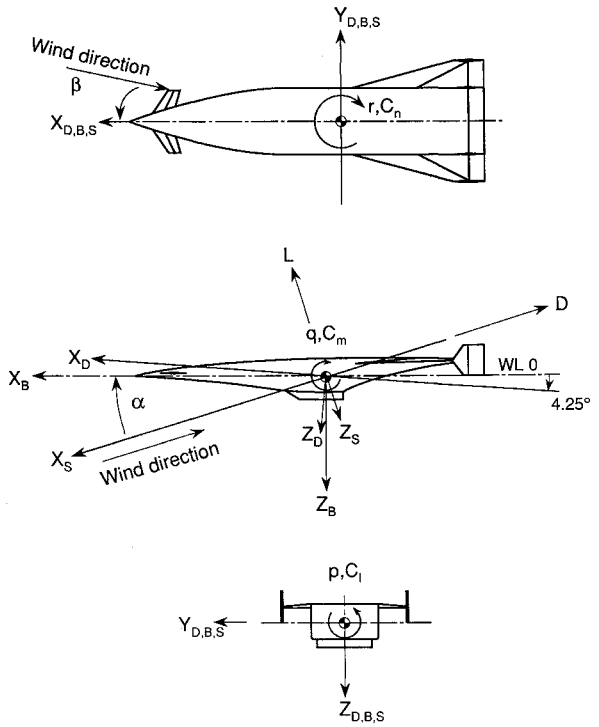

Fig. 1 Systems of axes used in investigation. Arrows indicate positive direction of moments, forces, and angles.

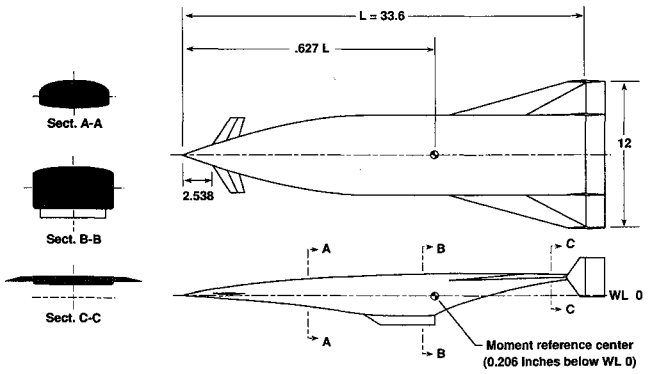

Fig. 2 Model geometry. Linear dimensions are in inches.

Model

A sketch of the TTD configuration (including all components) is presented in Fig. 2. The baseline configuration is the body, wings, outboard vertical tails, and nacelle. The wings have a 75-deg leading-edge sweep, an aspect ratio of 0.89, a taper ratio of 0.13, and a flat bottom with a half-diamond airfoil section on top. The half-diamond section is 3% thick with the maximum thickness at the 50% chord location. The wings are mounted with the leading edge 1.5 deg down with respect to the fuselage reference line. Both the inboard and outboard vertical tails have a 35-deg leading-edge sweep, an aspect ratio of 1.22, and a taper ratio of 0.65. These vertical tails have a diamond airfoil section with the maximum thickness varying linearly from 6% thick at the 25% chord location at the tip, to 4% thick at the 50% chord location at the root. The vertical tails are also mounted at a −1.5-deg angle with respect to the fuselage reference line. The canards have a 35-deg leading-edge sweep, an aspect ratio of 3.49, and a taper ratio of 0.45. The canards also have 4% thick diamond airfoil sections with the maximum thickness located at 50% of the local chord. The length of the wedge-shaped body flap is about 4.8% of the model reference length, and the width is about 54.9% of the model span. The body flap is deflected 10 deg trailing-edge down with respect to the lower surface of the model at the model trailing edge. The rectangular-shaped flow-through nacelle has a varying internal duct area along its length. The sidewalls of the nacelle at the inlet have a 60-deg leading-edge sweep. In addition, the sidewalls and the bottom wall at the inlet have 60-deg chamfers perpendicular to the leading edges.

Test Description

The investigation was conducted in the LaRC 7- by 10-Foot High Speed Tunnel.[6] For the static portion of the tests, forces and moments were measured on a six-component strain-gauge balance mounted internally in the model. The test was conducted at Mach numbers of 0.3, 0.6, and 0.8 with corresponding Reynolds numbers of approximately 2, 3.5, and 4 × 10^6/ft, respectively. The models were tested over an angle-of-attack range from approximately −4 to 16 deg. The angles of attack and sideslip have been corrected for the effects of sting bending under load. Jet boundary and blockage corrections have been applied to the data. The balance chamber pressure and the model nacelle base pressures were measured. The axial force, normal force, and pitching moment were corrected to a condition of freestream static pressure acting over the chamber and base areas.

To ensure a turbulent boundary layer over the model, carborundum grit was applied as three-dimensional roughness to the model nose and near the leading edges of the canards, wings, vertical tails, and nacelle. The size and location of the grit were chosen based on the work in Ref. 7.

The dynamic stability tests were also conducted at Mach numbers of 0.3, 0.6, and 0.8. The principles of operation of the small-amplitude, forced oscillation dynamic stability balances are discussed in Refs. 8 and 9. For the pitch oscillation tests, the value of the reduced frequency parameter k varied from 0.0296 to 0.1295. During the yaw oscillation tests k varied from 0.0106 to 0.0393, and for the roll tests k varied from 0.0344 to 0.1059. These tests were conducted over an angle-of-attack range from −4 to 14 deg.

Experimental Results and Discussion

Static Results

The static and dynamic results focus on the baseline configuration and on the effects of canards, body flap, and vertical

tail spanwise location. The canard data are for a 0-deg deflection, and the body flap is deflected 10-deg trailing-edge down with respect to the lower surface of the model at the trailing edge.

The static longitudinal characteristics of the baseline configuration, *BWVN*, at 0.3, 0.6, and 0.8 Mach numbers are shown in Fig. 3. The pitching moment for a given Mach number has a stable variation with angle of attack and is almost linear at the lower angles of attack. The results are dependent

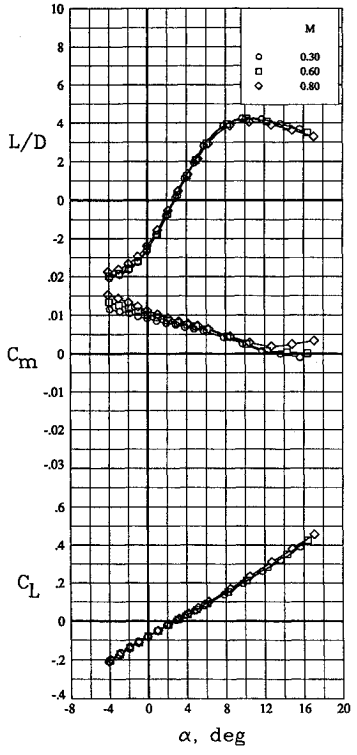

Fig. 3 Effect of Mach number on the static longitudinal characteristics of the *BWVN* configuration.

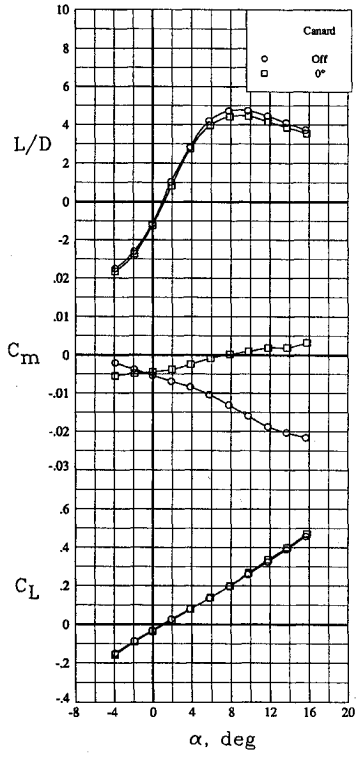

Fig. 4 Effect of the canard on the static longitudinal characteristics of the *BWVNF* configuration at 0.3 Mach number.

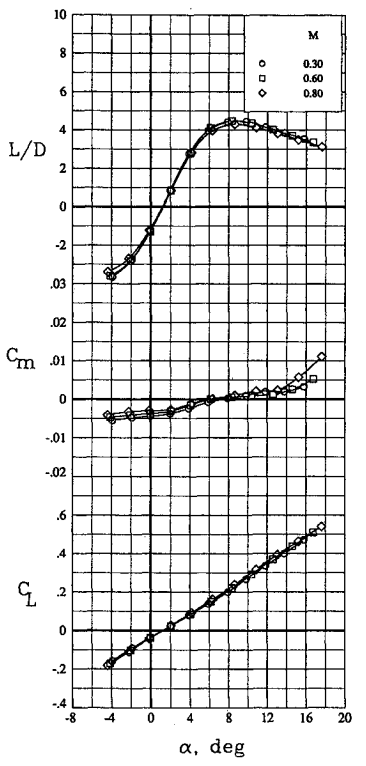

Fig. 5 Effect of Mach number on the static longitudinal characteristics of the *BWVNCF* configuration.

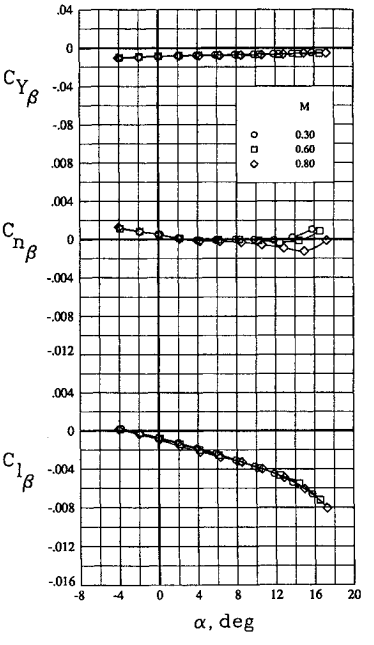

Fig. 6 Effect of Mach number on the static lateral-directional characteristics of the *BWVN* configuration.

on Mach number in that the level of stability increases with Mach number at the lower angles of attack. Also, at Mach 0.8 the stability is negative above about 12-deg angle of attack. Figure 4 shows the effect of the canard on the baseline configuration with the body flap at 0.3 Mach number. Adding the canard does change the static pitch stability from positive to negative, but there is a trim point at 8-deg angle of attack. The effect of Mach number on the baseline configuration with the canard and body flap is shown in Fig. 5. The trim angle of attack of 8 deg is not affected by Mach number and occurs at the maximum *L/D*.

The static lateral-directional characteristics for the baseline configuration are presented in Fig. 6. The rolling moment and

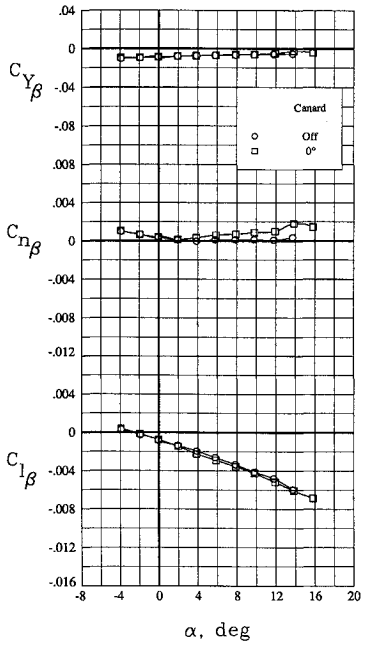

Fig. 7 Effect of the canard on the static lateral-directional characteristics of the *BWVNF* configuration at 0.3 Mach number.

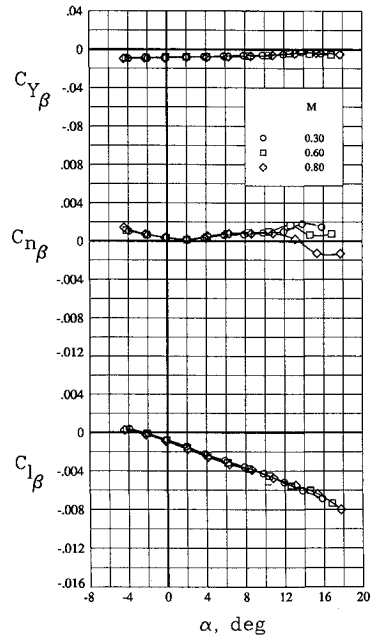

Fig. 8 Effect of Mach number on the static lateral-directional characteristics of the *BWVNCF* configuration.

side force derivatives show little variation with Mach number. The directional stability is positive between −4 and 2-deg angle of attack, but the stability is dependent on Mach number above about 8 deg. Figure 7 shows the effect of adding the canard to the baseline configuration with the body flap at 0.3 Mach number. The canard is seen to increase the directional stability above 3-deg angle of attack. Figure 8 shows the Mach number effect on the basic configuration with the canard and the body flap. The directional stability does change with Mach number above 10-deg angle of attack, and at 0.8 Mach number the directional stability is negative above 14-deg angle of attack.

Dynamic Results

Pitching Characteristics

The oscillatory stability parameters measured during the pitching oscillation tests are presented in Fig. 9 for the three Mach numbers. The upper portions of Figs. 9a, 9b, and 9c show the effect of TTD configuration change on the damping-in-pitch parameter. Negative values of the parameter represent stable damping in pitch. The baseline configuration, *BWVN*, has an almost constant level of pitch damping over this angle-of-attack range of about −4 to 14 deg. The addition of the canard to the baseline configuration slightly increases the pitch damping up to about 12-deg angle of attack, but the pitch damping decreases to the level of the baseline configuration above that angle of attack. Adding the body flap with the canard gave only a small additional increase in pitch damping. Moving the vertical tails to the inboard position, *BWV2N*, resulted in only a very slight decrease in damping compared to the baseline configuration.

The lower portions of Figs. 9a, 9b, and 9c contain the results for the oscillatory longitudinal-stability parameter. The baseline configuration has stable values of this parameter, but at

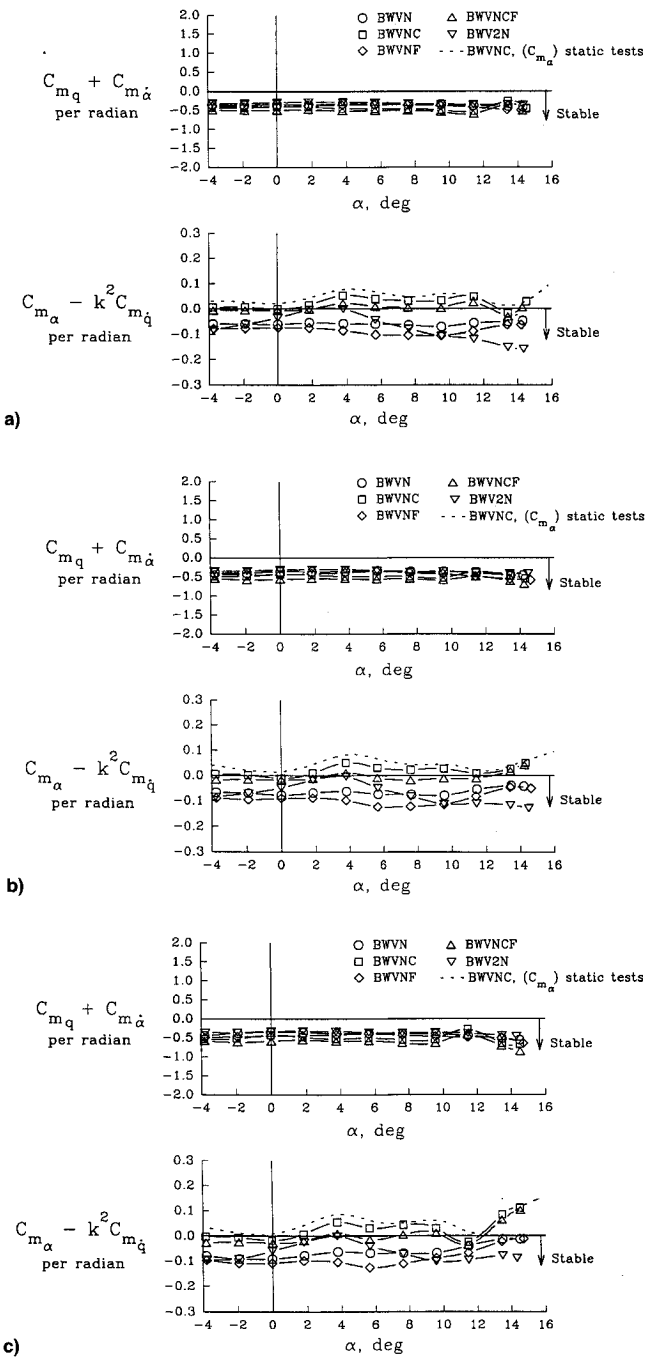

Fig. 9 Effect of canards, body flap, and vertical tail spanwise location on the damping-in-pitch parameter and the oscillatory longitudinal-stability parameter. *M* = a) 0.3, b) 0.6, and c) 0.8.

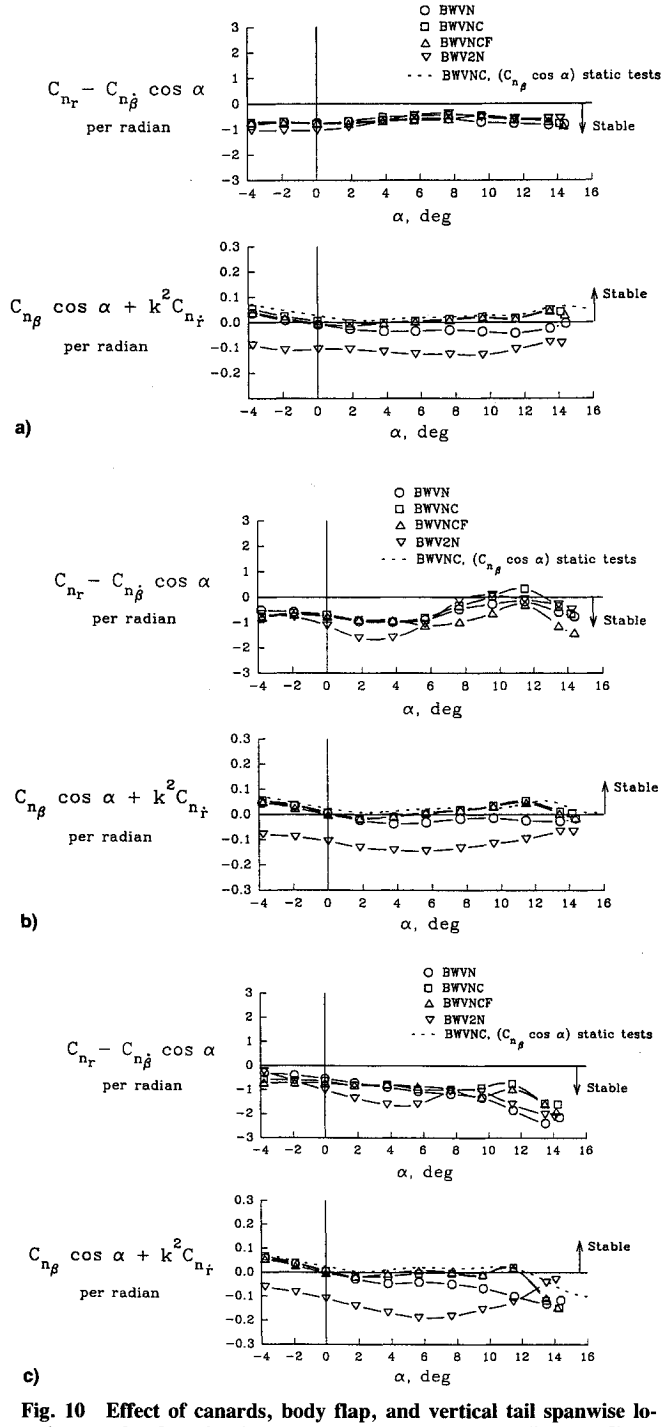

Fig. 10 Effect of canards, body flap, and vertical tail spanwise location on the damping-in-yaw parameter and the oscillatory directional-stability parameter. M = a) 0.3, b) 0.6, and c) 0.8.

Mach 0.8 the parameter approaches the unstable region at the higher angles of attack. Adding the canard to the baseline configuration changes the oscillatory longitudinal-stability parameter to near neutral or unstable values. A comparison of C_{m_α} computed from the static test results with the oscillatory longitudinal-stability parameter is also shown in the lower portions of Figs. 9a, 9b, and 9c. This comparison is for the baseline configuration plus canard and shows good agreement between the static and dynamic results. This good agreement demonstrates that the dynamic stability measurement technique is working properly. The use of the body flap generally increased the level of the longitudinal-stability parameter. Moving the vertical tails to the inboard position made the longitudinal-stability parameter nonlinear with angle of attack.

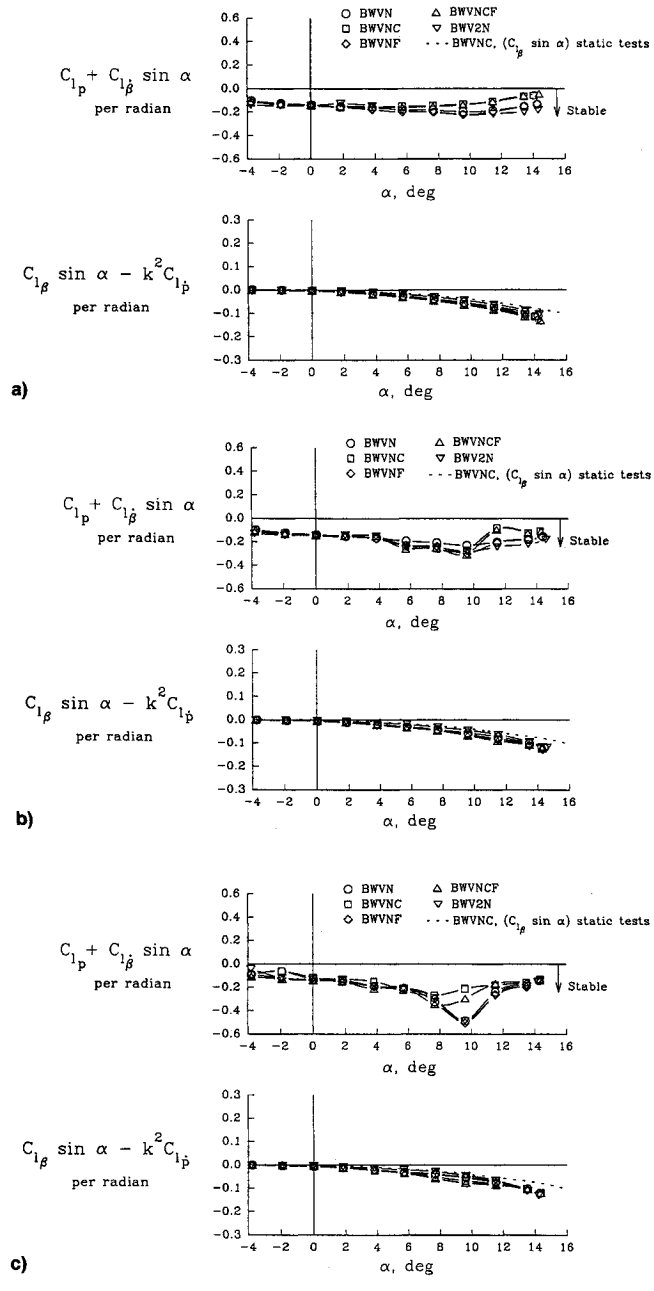

Fig. 11 Effect of canards, body flap, and vertical tail spanwise location on the damping-in-roll parameter and the rolling moment due to roll displacement parameter. M = a) 0.3, b) 0.6, and c) 0.8.

Yawing Characteristics

The oscillatory stability parameters measured during the yawing oscillation tests are contained in Fig. 10. The baseline configuration has stable damping in yaw (negative values of the parameter $C_{n_r} - C_{n_{\dot\beta}}$ cos α) over the range of angle of attack and Mach number as seen in the upper portions of Figs. 10a, 10b, and 10c. However, the yaw damping does decrease to a near zero value between 11- and 12-deg angle of attack at Mach 0.6 in Fig. 10b. Adding the canard had the effect of decreasing the damping in yaw above 8-deg angle of attack. Negative damping was measured for the configuration with the canard at about 11.5-deg angle of attack at Mach 0.6. Reference 10 discusses a similar reduction in yaw damping when adding canards to a conical aerospace plane concept tested at subsonic speeds. This reference states that while the addition of canards can enhance the directional-stability characteristics at high angles of attack by altering the forebody flowfield, this same flowfield change may reduce the level of yaw damping. The same is generally true for the present results.

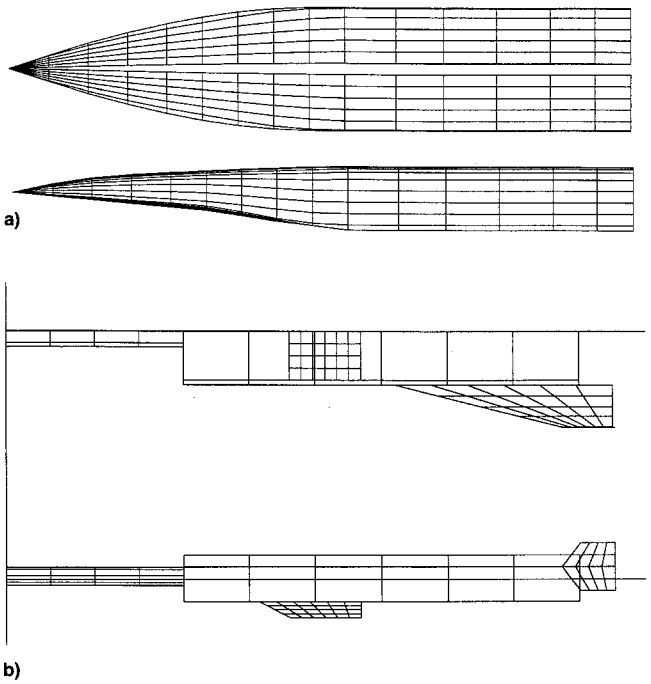

Fig. 12 APAS models of TTD: a) slender body component of TTD body and b) interference shell component model.

At low positive angles of attack, the configuration with the inboard vertical tails has more damping than the baseline configuration (with the vertical tails at the wingtips). Above 6 to 8 deg the opposite was true and the baseline configuration has more damping in yaw.

The lower portions of Figs. 10a, 10b, and 10c show the results for the oscillatory directional-stability parameter. These results indicate that the baseline configuration has stable values only at negative angles of attack. The addition of the canard generally improves the directional-stability parameter at angles of attack of 4 deg and higher. A similar result was observed in the static test results. This improvement from the canard tends to disappear at the highest angles of attack. There is a large degradation in the directional stability when the vertical tails are in the inboard position. There is an exception at 0.8 Mach number at the highest angles of attack where the configuration with inboard vertical tails is more stable than the baseline configuration. A comparison of C_{n_β} cos α computed from the static test results is also contained in the lower portions of Figs. 10a, 10b, and 10c. To make a proper comparison, the static data were transferred to the axis system used for the dynamic stability parameters. There is very good agreement between the static and dynamic results except at the highest angles of attack at 0.8 Mach number.

Rolling Characteristics

The oscillatory stability parameters measured during the rolling oscillation tests are shown in Fig. 11. The roll damping of the various configurations is contained in the upper portions of Figs. 11a, 11b, and 11c. All of the configurations have stable values of the roll damping parameter. There is a distinct peak in the damping just below 10-deg angle of attack for the baseline configuration and for the other configurations without the canard. The primary configuration component to have an effect on the roll damping is the canard. Adding the canard to the baseline configuration decreased the roll damping over some portion of the angle-of-attack range depending on the Mach number.

The bottom portions of Figs. 11a, 11b, and 11c show the effect of the canard, body flap, and vertical tail spanwise location on the rolling moment due to roll-displacement parameter. The first term in this parameter, C_{l_β} sin α, is the aerodynamic "spring" term resulting from the rolling motion

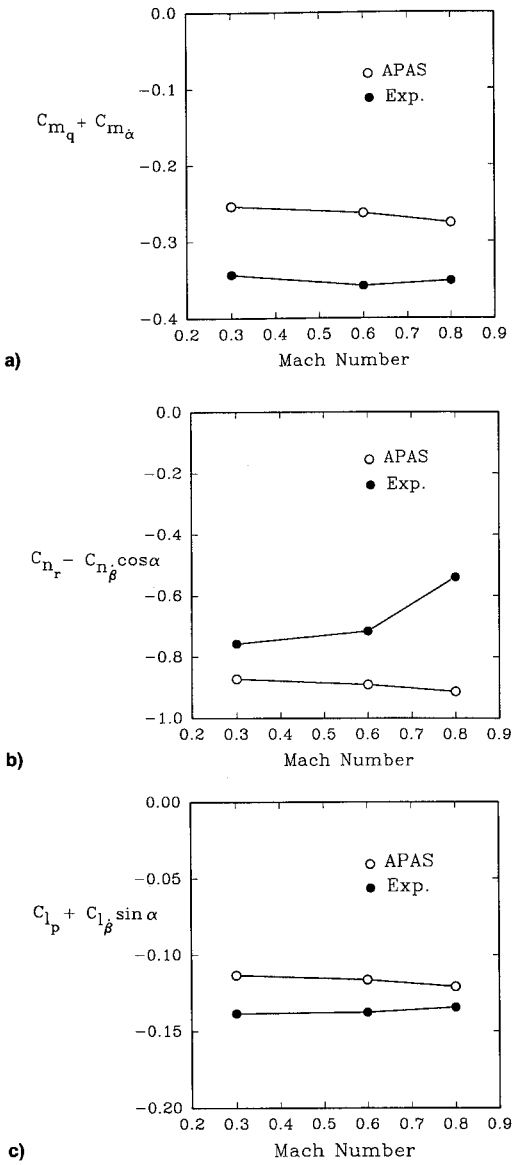

Fig. 13 Comparison of APAS results with experimental damping results: a) pitch, b) yaw, and c) roll damping comparisons.

about the body axis at angle of attack. This parameter is only minimally affected by the addition of the canards and body flap or by the vertical tail location. There is good agreement between the static and dynamic results up to about 10 deg and fair agreement at the higher angles of attack.

APAS Description

The APAS is an interactive computer program that allows an experienced user to quickly estimate aerodynamic forces and moments of arbitrary aerospace vehicles. The APAS uses a single geometry definition to approximate configuration aerodynamics throughout the speed range, including effects of control surfaces, ground effects, landing gear, high altitudes, and dynamic damping.

At subsonic and low supersonic speeds, the APAS utilizes a combination of slender body theory, empirical viscous and base drag values, a theoretical wave drag calculation, and source and vortex panel distributions. Detailed information concerning the APAS, including program formulation and comparisons with experimental data and CFD results, can be found in Refs. 3, 4, and 11–16.

APAS Analysis of the TTD

The APAS was used to estimate damping derivatives (C_{m_q}, C_{n_r}, and C_{l_p}) for the baseline configuration (*BWVN*). Figure

12a illustrates the TTD body as modeled and analyzed using the slender body component of APAS. Past experience with NASP configurations has shown that much better results are obtained if the body cross section is held constant over the rear half of the body as seen in the side view. Figure 12b shows how the interference shell component modeled the TTD. At each tunnel condition, four separate APAS analyses were performed (one analysis with no vehicle rotation, and one each with p, q, and r equal to one rad/s). The rotation rates p, q, and r entered the APAS calculation process as local velocity increments. The moment increments used in calculating the dynamic damping derivatives were then calculated by differencing two APAS results (one with a one rad/s rotation and one with no vehicle rotation).

Comparison of APAS Results with Wind-Tunnel Data

Dynamic damping derivative estimates from the APAS for a conical aerospace plane configuration have been compared to wind-tunnel data in the past, but only in the low subsonic speed range.[11] Comparisons of the present results for the baseline configuration are shown in Fig. 13. The experimental values used in the figures are at 0-deg angle of attack. Note that APAS can estimate only the first of the two combined terms in each of the damping parameters. The APAS predictions for the pitch damping were 22–27% lower than the experimental values. The APAS yaw damping overpredicted the experimental values by 15–69%. The APAS roll damping estimates were 10–18% lower than the experimental values. Based on these percentage differences, the APAS damping predictions are considered to be good for the roll mode and only fair for the pitch and yaw modes for this configuration. As shown in Refs. 11–16, however, good agreement between APAS results and static wind-tunnel data is often encountered throughout the angle-of-attack and Mach number ranges.

Summary of Results

Static and dynamic tests were made to determine the aerodynamic characteristics of an LaRC designed blended body NASP configuration designated the TTD. The small-amplitude, forced-oscillation dynamic stability technique was successfully used to test this nonpowered configuration in the pitch, yaw, and roll modes at subsonic speeds. The static and dynamic tests were made over a range of Mach numbers of 0.3, 0.6, and 0.8, and over a range of angles of attack from −4 to 16 deg. The results are summarized as follows:

1) The baseline configuration has positive static stability except at the higher angles of attack at 0.8 Mach number.

2) Adding a canard to the baseline configuration changes the static stability from positive to negative.

3) The baseline configuration has negative directional stability at moderate positive angles of attack.

4) The addition of a canard to the baseline configuration improves the directional stability.

5) The baseline configuration has positive damping in the pitch, yaw, and roll modes.

6) The APAS damping predictions for the baseline configuration are considered to be good for the roll mode and only fair for the pitch and yaw modes.

References

[1]Harris, R. V., Jr., "On the Threshold—The Outlook for Supersonic and Hypersonic Aircraft," AIAA Paper 89-2071, July 1989.

[2]Sanchez, F., "The National Aero-Space Plane, the Guidance and Control Engineer's Dream or Nightmare?" *Proceedings of the Annual Rocky Mountain Guidance and Control Conference* (Keystone, CO), *Guidance and Control 1989*, Vol. 68, Advances in the Astronautical Sciences, AAS 89-040, 1989, pp. 339–352.

[3]Bonner, E., Clever, W., and Dunn, K., "Aerodynamic Preliminary Analysis System II. Part I—Theory," NASA CR-182076, April 1991.

[4]Sova, G., and Divan, P., "Aerodynamic Preliminary Analysis System II. Part II—User's Manual," NASA CR-182077, April 1991.

[5]Dress, D. A., Boyden, R. P., and Cruz, C. I., "Supersonic Dynamic Stability Characteristics of the Test Technique Demonstrator NASP Configuration," AIAA Paper 92-5009, Dec. 1992.

[6]Fox, C. H., Jr., and Huffman, J. K., "Calibration and Test Capabilities of the Langley 7- by 10-Foot High Speed Tunnel," NASA TM X-74027, May 1977.

[7]Braslow, A. L., and Knox, E. C., "Simplified Method for Determination of Critical Height of Distributed Roughness Particles for Boundary-Layer Transition at Mach Numbers from 0 to 5," NACA TN-4363, Sept. 1958.

[8]Braslow, A. L., Wiley, H. G., and Lee, C. Q., "A Rigidly Forced Oscillation System for Measuring Dynamic-Stability Parameters in Transonic and Supersonic Wind Tunnels," NASA TN D-1231, March 1962.

[9]Freeman, D. C., Boyden, R. P., and Davenport, E. E., "Supersonic Dynamic Stability Characteristics of a Space Shuttle Orbiter," NASA TN D-8043, June 1976.

[10]Hahne, D. E., Riebe, G. D., Riley, D. R., and Pegg, R. J., "Exploratory Wind-Tunnel Investigation of the Low-Speed Aerodynamic Characteristics of a Conical Aerospace Plane Concept," NASA TP 2860, Jan. 1989.

[11]Hahne, D. E., Luckring, J. M., Covell, P. F., Phillips, W. P., Gatlin, G. M., Shaughnessy, J. D., and Nguyen, L. T., "Stability Characteristics of a Conical Aerospace Plane Concept," Society of Automotive Engineers, SAE-892313, Sept. 1989.

[12]Cruz, C., and Wilhite, A., "Prediction of High-Speed Aerodynamic Characteristics Using the Aerodynamic Preliminary Analysis System (APAS)," AIAA Paper 89-2173, July 1989.

[13]McCandless, R., and Cruz, C., "Hypersonic Characteristics of an Advanced Aerospace Plane," AIAA Paper 85-0346, Jan. 1985.

[14]Blosser, M., Scotti, S., Cerro, J., Powell, R., Jackson, L. R., and Cruz, C., "Design Study of a Slant-Nose-Cylinder Aeroassisted Transfer Vehicle," AIAA Paper 85-0966, June 1985.

[15]Phillips, W. P., and Cruz, C., "Super/Hypersonic Aerodynamic Characteristics for a Transatmospheric Vehicle Concept Having a Minimum Drag Forebody," AIAA Paper 91-1694, June 1991.

[16]Cruz, C., and Ware, G., "Predicted Aerodynamic Characteristics for HL-20 Lifting-Body Using the Aerodynamic Preliminary Analysis System (APAS)," AIAA Paper 92-3941, July 1992.